Tracking Attracting Manifolds in Flows

Dhanushka Kularatne ·
M. Ani Hsieh

Abstract This paper presents a collaborative control strategy designed to enable a team of robots to track attracting Lagrangian coherent structures (LCS) and unstable manifolds in two-dimensional flows. Tracking LCS in flows is important for many applications such as planning energy optimal paths in the ocean and for predicting the evolution of various physical and biological processes in the ocean. The proposed strategy which tracks attracting LCS and unstable manifolds in real-time through direct computation of the local finite time Lyapunov exponent field, does not require global information about the dynamics of the surrounding flow, and is based on local sensing, prediction, and correction. The collaborative control strategy is implemented on a team of robots and theoretical guarantees for the tracking and formation keeping strategies are presented. We demonstrate the performance of the tracking strategy in simulation using actual ocean flow data and experimental flow data generated in a tank. The strategy is validated experimentally using a team of micro autonomous surface vehicles (mASVs) in an actual fluid environment.

Keywords Marine Robotics · Manifold Tracking · LCS · Distributed Robot Systems

Dhanushka Kularatne
Scalable Autonomous Systems Lab, Drexel University, Philadelphia
Tel.: +1-469-200-9338
E-mail: dnk32@drexel.edu

M. Ani Hsieh
Scalable Autonomous Systems Lab, Drexel University, Philadelphia
Tel.: +1-215-895-5803
E-mail: mah349@drexel.edu

1 Introduction

We are interested in the development of collaborative control strategies for distributed sensing and tracking of coherent structures and manifolds in flows using teams of autonomous underwater and surface vehicles (AUVs and ASVs). Specifically, we are interested in deploying teams of robots to track a class of coherent structures that are important for quantifying transport phenomena in flows.

Inanc *et al.* showed that time and fuel optimal paths in the ocean can coincide with a specific class of coherent structures called Lagrangian coherent structures (LCS) (Inanc et al., 2005; Senatore and Ross, 2008). LCS are the extensions of stable and unstable manifolds to general time dependent flows (Haller and Yuan, 2000; Haller, 2011) and are similar to separatrices that divide the flow into dynamically distinct regions. This is supported by Forgoston *et al.*'s work where they showed that LCS coincide with regions in the flow field where more escape events occur (Forgoston et al., 2011). Furthermore, it has been shown that biological phenomena in the ocean, such as the dispersion of algea blooms, can be predicted using knowledge about propagation of LCS boundaries (Olascoaga et al., 2008). More importantly, Olascoaga *et al.* have shown that, the class of LCS that we are interested in *i.e., attracting* LCS, was responsible for pushing spilled oil from the Deepwater Horizon spill in 2010, towards the coast of Florida (Olascoaga and Haller, 2012). As such, knowledge of LCS is important for planning energy efficient trajectories in the ocean, maintaining sensors in their desired monitoring regions (Mallory et al., 2013; Hsieh et al., 2014; Heckman et al., 2014), predicting pollutant dispersion and for enabling efficient, computationally tractable estimation and prediction of the underlying geophysical fluid dynamics.

Existing methods require complete knowledge of the underlying flow field to numerically compute and track the location of an LCS in a flow. However, accessibility to and the overall quality of ocean current hindcasts, nowcasts, and forecasts provided by Navy Coastal Ocean Model (NCOM) databases (SCRIPPS, 2014), regional ocean model systems (ROMS) (Smith et al., 2010), and/or other numerical models are generally low. This is because most existing ocean models are derived from assimilated satellite and field data with predictions from numerical PDE models (Shchepetkin and McWilliams, 1998, 2005). As such, existing data sets that describe ocean flows are mostly finite time, of low spatiotemporal resolution and are limited to specific regions. Due to this sparseness of available ocean data, locating and tracking LCS in real time is problematic. In this paper we seek to establish a methodology that will enable a team of ASV's to track an attracting LCS in real time, using on board flow velocity measurements. To the best of our knowledge this is

the first instance where direct on board flow measurements have been used locate and track LCS.

In two-dimensional (2D) flows, LCS are one-dimensional separating boundaries analogous to ridges defined by local maximum instability, and can be quantified by local measures of Finite-Time Lyapunov Exponents (FTLE) (Shadden et al., 2005). The tracking of coherent structures in fluids is challenging since the structures are generally unstable and time dependent. Existing work have shown that it is possible to use a team of robots to collaboratively track the stable manifolds and LCS boundaries in 2D flows (Michini et al., 2014a,c,b). The strategy relies on robots maintaining a boundary saddling formation while collecting local measurements of the flow velocity. LCS tracking is achieved by fusing the data to identify the region in the flow field with the extremal velocity.

While the strategy has been validated using analytical models that describe large scale ocean circulation (Hsieh et al., 2012; Michini et al., 2014c), experimental data created in a flow tank, actual ocean data (Michini et al., 2014a), and a scaled robotic platform (Michini et al., 2014b), the work is focused on tracking the repelling LCS boundaries or stable manifolds in 2D flows. Since the identification of repelling LCS boundaries requires the computation of forward FTLEs, real-time tracking of the LCS boundaries in these existing work is achieved by solely examining the flow velocities in the region spanned by the robot team and do not rely on actual FTLE computations. As such, no explicit information can be obtained about the type of the LCS boundary being tracked. Lastly, since the LCS boundaries are not explicitly resolved, the team of robots may end up tracking a *non-existent* boundary.

In this work, which is an extension of the work in (Kularatne and Hsieh, 2015), we present a methodology to track attracting LCS boundaries and unstable manifolds through the explicit on-board calculation of local FLTE fields. This can be done in real-time since the required FTLE calculations only use previously acquired flow velocity data. The proposed tracking strategy utilizes the FTLE field along with instantaneous local flow field measurements to resolve the attracting LCS boundary. Different from the work in (Kularatne and Hsieh, 2015), in this work we

(a) present a formation keeping strategy that is more robust to measurement uncertainty,
(b) analyze the tracking and formation keeping strategies to provide theoretical performance guarantees, and
(c) validate the strategy using actual ocean flow data and flow data generated in an experimental flow tank.

The remainder of this paper is structured as follows. We provide a background on characterizing LCS using local FTLE measures and then formulate the problem in Section 2. The development of the proposed control strategy is presented in

Section 3 and its theoretical feasibility is analyzed in Section 4. Simulation and experimental results are presented in Section 5 and Section 6 respectively. We conclude with a discussion of our results and directions for future work in Section 7.

2 Background and Problem statement

2.1 Background

In this paper we consider the problem of tracking an attractive Lagrangian Coherent Structure (LCS) in a 2D planar flow field of the form

$$\dot{\mathbf{x}}(t) = \mathbf{F}(\mathbf{x}, t) \tag{1}$$

where $\mathbf{x} = [x, y]'$ gives the position in the plane with respect to some inertial frame $\mathbf{O}$ and $\mathbf{x}'$ denotes the transpose of the vector $\mathbf{x}$.

The position of a fluid particle advected by the flow field given by (1), is a function of time t, the starting point of the particle $\mathbf{x_0}$ and starting time t_0, *i.e.,* $\mathbf{x} = \mathbf{x}(t; \mathbf{x_0}, t_0)$. Using the notation used by Shadden *et al.* (Shadden et al., 2005), the solution to the dynamical system given in (1) can be viewed as a flow map which takes points from their initial position $\mathbf{x_0}$ at time t_0 to their position at time t. This map, denoted by $\phi_{t_0}^t$, satisfies

$$\phi_{t_0}^t(\mathbf{x_0}) = \mathbf{x}(t; \mathbf{x_0}, t_0), \tag{2}$$

and has the properties $\phi_{t_0}^{t_0}(\mathbf{x}) = \mathbf{x}$ and $\phi_{t_0}^{s+t}(\mathbf{x}) = \phi_s^{s+t}(\phi_{t_0}^s(\mathbf{x}))$. The Finite Time Lyaponov Exponent (FTLE) over a finite integration time interval T, associated with a point $\mathbf{x}$ at time t_0 is given by,

$$\sigma_{t_0}^T(\mathbf{x}) = \frac{1}{|T|} ln \sqrt{\lambda_{max}(\Delta)} \tag{3}$$

where $\lambda_{max}(\Delta)$ is the maximum eigenvalue of the finite-time version of the Cauchy-Green deformation tensor Δ, given by,

$$\Delta = \frac{d\phi_{t_0}^{t_0+T}(\mathbf{x})}{d\mathbf{x}}' \frac{d\phi_{t_0}^{t_0+T}(\mathbf{x})}{d\mathbf{x}}. \tag{4}$$

The value of Δ is computed numerically by discretizing the domain into a regular grid and computing the trajectories of each point and its immediate neighbors in the grid from time t_0 to $t_0 + T$ by numerically integrating (1) (see Fig. 1(a)).

In this paper, LCS are considered to be ridges in the FTLE field calculated using (3), *i.e.,* maximal values in the FTLE field, as defined by Shadden *et al.* (Shadden et al., 2005). The *forward-time* FTLE field calculated by advecting fluid particles forward in time ($T > 0$), reveals repelling LCS which are analogous to the stable manifolds of saddle points in a time independent flow field. Conversely, the

backward-time FTLE field ($T < 0$) reveals attracting LCS which are analogous to unstable manifolds of a time independent flow field. Fig. 2 shows the forward and backward time FTLE fields computed for a time independent flow field generated using the wind driven double gyre model.

The FTLE value gives a measure of the maximum expansion of two initially nearby particles when they are advected by the flow. Therefore, particles initiated on opposite sides of an LCS will have much higher FTLE values than their neighbors, since an LCS acts as a boundary between two dynamically distinct regions of the flow (Shadden et al., 2005). Thus, by calculating the FTLE field in a neighborhood that contains an LCS, it should be possible to find the LCS boundary by tracing out points with the highest FTLE values.

2.2 Problem Statement

Let B_u denote an attractive LCS of the flow field given in (1). Since $\mathbf{F}(\mathbf{x},t)$ is a 2D flow field, B_u will be a time varying 1D curve in the domain of $\mathbf{F}$. In this work, a team of N Autonomous Surface Vehicles (ASVs) are used to track B_u in real-time. Each ASV is assumed to have the kinematic model given by,

$$\dot{x}_i = V_i \cos \theta_i + u_i \tag{5a}$$
$$\dot{y}_i = V_i \sin \theta_i + v_i \tag{5b}$$
$$\dot{\theta}_i = \omega_i \tag{5c}$$

where V_i is the speed of the ith ASV (P_i) with respect to the flow, θ_i is its heading direction, $\mathbf{x}_i = [x_i, y_i]'$ is its position with respect to the inertial frame $\mathbf{O}$ and $[u_i, v_i]' = \mathbf{F}(\mathbf{x_i}, t)$ is the velocity of the underlying flow field at $\mathbf{x_i}$. The control inputs of the ith ASV are V_i and ω_i. In vector form, the velocity of P_i could be written as,

$$\dot{\mathbf{x}_i}(\mathbf{x_i}, t) = \mathbf{V_{i/f}}(t) + \mathbf{F}(\mathbf{x_i}, t) \tag{6}$$

where $\mathbf{V_{i/f}}$ is the velocity of P_i relative to the flow. Note that V_i and θ_i are the magnitude and direction of $\mathbf{V_{i/f}}$ respectively. We assume that each ASV has the capability to measure the flow velocity at its current position and that each ASV can communicate bi-directionally with a data processing vehicle. Throughout this work, we assume that the ASVs are initialized with the center ASV (P_c), coincident on B_u as shown in Fig. 1(b). Using the definitions and assumptions given above, we can now state the problem being addressed in this paper as follows:

"Given an estimate for the position of a point on B_u at time t_0, develop a collaborative control strategy to track B_u for time $t > t_0$ for a team of ASVs with the kinematic model given by (5)."
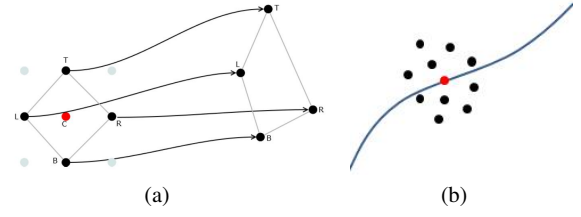

Fig. 1 (a) Locations of neighboring particles for the numerical computation of Δ, (b) Agents are initialized with the center agent of the grid coincident on the attracting LCS
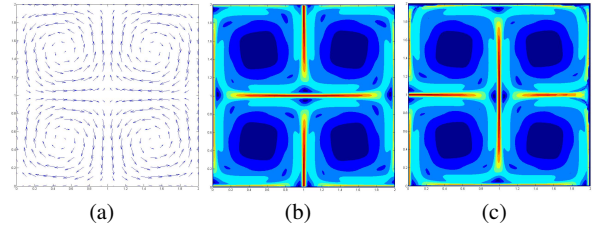

Fig. 2 (a) Time independent flow field generated using the wind driven double gyre model. A saddle point can be observed at (1,1). Though not clearly seen additional saddle points exist at (0,0), (0,1), (0,2), (1,0), (1,2), (2,0), (2,1) and (2,2), (b) Forward time FTLE field which reveals the stable manifolds. (c) Backward time FTLE field which reveals the unstable manifolds

3 Methodology

In the proposed methodology, the center ASV P_c is tasked with tracking the boundary B_u, *i.e.*, the trajectory of P_c will give the time evolution of a point on B_u. The other ASVs in the sensing grid are required to maintain formation around P_c so that valid flow measurements are available for computing and tracking the boundary. In the proceeding sections, the position of P_c at time t is given by $\mathbf{x_c}(t) = [x_c, y_c]'$.

3.1 Manifold Tracking

The methodology proposed in this paper utilizes a combination of *backward-time* FTLE computations and the PIM triple inspired tracking strategy (Hsieh et al., 2012) to locate the attractive LCS boundary.

3.1.1 Locating the LCS boundary using the FTLE field

Considering the flow velocity measurements obtained by the team of ASVs, an approximation could be obtained for the velocity field given in (1) as

$$\dot{\hat{\mathbf{x}}}(t) = \hat{\mathbf{F}}(\mathbf{x}, t) \tag{7}$$

for $t = t_0, ..., t_i, ..., t_f$ and $\mathbf{x} = \mathbf{x_1^0}, \mathbf{x_2^0}, ..., \mathbf{x_N^0}, ..., \mathbf{x_1^f}, \mathbf{x_2^f}, ..., \mathbf{x_N^f}$, where t_i is the ith sampling instance and $\mathbf{x_j^i}$ is the position of the jth ASV at t_i. In order to calculate the *backward-time*

FTLE field around the center agent, a set of fluid particles arranged in a grid around P_c are advected along the flow backwards in time. This is achieved by integrating the particle positions backwards in time using $\hat{\mathbf{F}}$, *i.e.,* $T < 0$. The resulting flow map is used in (4) and (3) to compute the *backward-time* FTLE field on this grid. To overcome the inherent sparseness of the available measurements, trilinear interpolation is used on $\hat{\mathbf{F}}$ to approximate the flow velocities at spatio-temporal coordinates for which direct velocity measurements are unavailable. The interpolation should not affect the accuracy of boundary extraction since it has been shown that FTLE maxima are relatively insensitive to the interpolation scheme used in their computations (Harrison and Glatzmaier, 2012) and that strong LCS are relatively robust to uncertainty (Lermusiaux and Lekien, 2005). Since we assume that P_c is initialized on B_u itself, following from the discussion in Section 2.1, the point with the highest FTLE value on this grid will correspond to a point on the LCS. Thus, the point with the highest FTLE value in the computed FTLE field is selected as the boundary location ($\mathbf{q_F}$) at the current sampling instance.

3.1.2 Locating the LCS boundary using the PIM inspired strategy

Since LCS are time varying, tracking based solely on FTLE computations will tend to fail, when the time scales of the past flow velocity measurements are not representative of the time scales of the current or future time variations of the boundary. To address this, we augment the FTLE based tracking strategy with the boundary tracking strategy introduced by Hsieh *et al.* (Hsieh et al., 2012) which is based on the PIM triple method (Nusse and Yorke, 1989). We briefly summarize the strategy below and refer interested readers to (Hsieh et al., 2012; Michini et al., 2014a) for more information.

Given a team of three robots, denoted $\{L; C; R\}$, robot C is tasked to remain close to the boundary of interest, *i.e.,* track B_u, while robots L and R are tasked to remain on opposite sides of B_u at all times. Thus the three robots will maintain a saddle straddle formation across the boundary at all times. Let $\hat{\mathbf{u}}_\mathbf{L}(t) = \hat{\mathbf{F}}(\mathbf{x_L}, t)$, $\hat{\mathbf{u}}_\mathbf{C}(t) = \hat{\mathbf{F}}(\mathbf{x_C}, t)$ and $\hat{\mathbf{u}}_\mathbf{R}(t) = \hat{\mathbf{F}}(\mathbf{x_R}, t)$ denote the flow velocity measurements obtained by L, C and R at their respective positions $\mathbf{x_L}$, $\mathbf{x_C}$ and $\mathbf{x_R}$ at time t. The saddle straddle line segment J whose end points are defined by $\mathbf{x_L}$ and $\mathbf{x_R}$, is discretized such that $\mathbf{x_L} = \mathbf{h_1} < \mathbf{h_2} < ... < \mathbf{h_M} = \mathbf{x_R}$. Given a set of velocity measurements $\hat{\mathbf{u}}_\mathbf{i}(t)$ and corresponding position estimates $\hat{\mathbf{x}}_\mathbf{i}(t)$, the flow velocity at $\mathbf{h_k}$ is calculated as

$$\mathbf{u}(\mathbf{h_k}) = \sum_j \sum_{i=1}^N \frac{w_{ij}\hat{\mathbf{u}}_\mathbf{i}(j)}{\sum_j \sum_{i=1}^N w_{ij}}$$

where $w_{ij} = \|\hat{\mathbf{x}}_\mathbf{i}(j) - \mathbf{h_k}\|^{-2}$. The location of the boundary on the current saddle straddle line segment is given by the point $\mathbf{h_B} = \arg\max_{k=1,...,M} \mathbf{u}(\mathbf{h_k})' \hat{\mathbf{u}}_\mathbf{c}(t)$.

The velocity measurements obtained by the team of ASVs is used with this method to compute the boundary location on a saddle straddle line segment defined by the two immediate neighbors of P_c on either side of the boundary. The boundary location found using the PIM triple based method is denoted by $\mathbf{q_P}$.

3.1.3 Boundary tracking

The boundary locations computed using the FTLE method and the PIM triple method are combined to get a better estimate of the actual boundary location ($\mathbf{q_h}$). Since P_c is tasked with tracking the boundary, any computed boundary location should be very close to the trajectory of P_c. Therefore, a distance based weighted averaging scheme is used to combine $\mathbf{q_F}$ and $\mathbf{q_P}$ to find a better approximation for the boundary location ($\mathbf{q_h}$). As such

$$\mathbf{q_h} = \frac{d_P \mathbf{q_F} + d_F \mathbf{q_P}}{d_P + d_F} \tag{8}$$

where d_F and d_P are the shortest distances from to $\mathbf{q_F}$ and $\mathbf{q_P}$ to the trajectory of P_c.

Next, the Lagrangian nature of the FLTE field is used to predict the future location of the LCS boundary. It has been shown by Shadden *et al.* (Shadden et al., 2005) that flux across an LCS is very small, *i.e.,* a particle on an LCS will remain on the LCS or remain very close to the LCS as it advects along the flow. Therefore, we advect a fluid particle located at $\mathbf{q_h}$ forward in time for T_1 seconds using $\hat{\mathbf{F}}$, to get an approximation of the future LCS location $\hat{\mathbf{q}}_\mathbf{h}$ as indicated in Fig. 3(a). Thus,

$$\hat{\mathbf{q}}_\mathbf{h} = \phi_t^{t+T_1}(\mathbf{q_h}) = \mathbf{q_h} + \int_t^{t+T_1} \hat{\mathbf{F}}(\mathbf{x}, t) dt. \tag{9}$$

In order for P_c to follow B_u, we want P_c to head towards $\hat{\mathbf{q}}_\mathbf{h}$ at all times, *i.e.,* we want the velocity of P_c in the inertial frame, $\mathbf{V_{gc}}$, to be directed towards $\hat{\mathbf{q}}_\mathbf{h}$ at all times. As shown in Fig. 3(b), this could be done by setting $\mathbf{V_{c/f}}$ (velocity of P_c relative to the flow) appropriately. Since we have the freedom to set $|\mathbf{V_{c/f}}|$ arbitrarily and set the direction θ_d accordingly, we select the minimum possible value for $|\mathbf{V_{c/f}}|$. It can be shown that this can be achieved by setting $\mathbf{V_{c/f}} = (u_i \sin\alpha - v_i \cos\alpha)\tilde{\mathbf{n}}$ where α is the desired direction of $\mathbf{V_{gc}}$ as shown in Fig. 3(b) and $\tilde{\mathbf{n}} = [-\sin\alpha, \cos\alpha]'$ is the direction normal to α. The corresponding $|\mathbf{V_{c/f}}|$ and θ_d are given by,

$$|\mathbf{V_{c/f}}| = |v_i \cos\alpha - u_i \sin\alpha| \tag{10a}$$

$$\theta_d = \alpha + \text{sign}\left(\mathbf{F}(\mathbf{x_c}, t) \times \mathbf{V_{gc}}\right)\frac{\pi}{2}. \tag{10b}$$
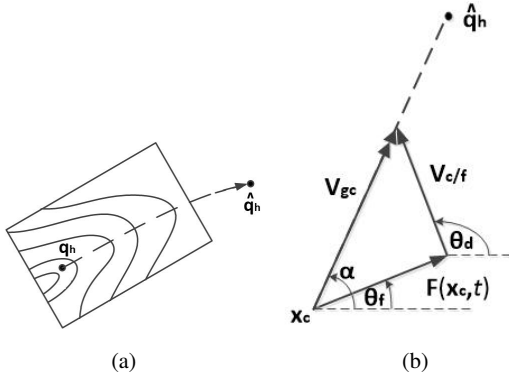
Fig. 3 (a) The LCS location $\mathbf{q_h}$ is detected on the calculated FTLE grid and the flow map is used to predict the future LCS location $\hat{\mathbf{q}}_{\mathbf{h}}$, (b) $\mathbf{V_{c/f}}$ is selected such that $\mathbf{V_{gc}}$ is always directed towards $\hat{\mathbf{q}}_{\mathbf{h}}$

Using (10), the velocity commands for P_c are set as,

$$V_c = |\hat{v}_i \cos\alpha - \hat{u}_i \sin\alpha| \tag{11a}$$
$$\omega_c = K_\omega (\theta_d - \theta_c) + \dot{\theta}_d \tag{11b}$$

where $\hat{u}_i = \hat{F}_x(\mathbf{x_c}, t)$, $\hat{v}_i = \hat{F}_y(\mathbf{x_c}, t)$ and θ_c is the current heading angle of P_c.

Remark 1

The proposed tracking strategy fundamentally relies on the team's ability to simultaneously measure the flow field on opposite sides of B_u. Thus, it is possible track the LCS using a minimum of three agents. However, the spatial spread of the flow data collected with just three agents would not be sufficient for effective FTLE calculations.

3.2 Formation Keeping

In order to accurately locate the boundary using *backward-time* FTLE calculations and to accurately predict the future LCS location, it is important that the flow velocity measurements available for these calculation are an accurate representation of the underlying flow field. As such, we require that the agents in the sensing grid

(a) maintain a boundary straddling formation, and
(b) maintain a sufficient spread across the boundary so as to capture the salient features of the flow across the boundary.

To achieve this, in our previous work (Kularatne and Hsieh, 2015), we proposed a formation keeping strategy that utilizes the attracting property of the boundary to maintain a grid formation across the boundary. Even though this strategy was verified in simulations and experiments, the stability of the formation and consequently the accuracy of

the FTLE computations depended significantly on the accuracy of the velocity measurements obtained by the team, *i.e.,* when measurement noise was high, the team lost the boundary straddling formation and this lead to inaccurate FTLE computations. Furthermore, that strategy was geared exclusively for rectangular formations and was not scalable for large numbers of sensing agents. In this work, to address these issues and to be able to vary the spread of the sensing grid to adapt to changing flow conditions, we use a formation keeping strategy that controls the mean (μ) and variance (ς^2) of the sensing grid. (Note the use of non-standard notation for the variance to distinguish it from the notation used for the FTLE in (3)).

If we control the mean of the grid such that it follows the trajectory of the center agent and if we control the variance of the grid to suit the flow characteristics, both (a) and (b) above are addressed. In addition, if the agent level controls are derived in terms of these group parameters, we address scalability issues as well. To achieve this, we use the group abstraction control strategy introduced by Belta *et al.* (Belta and Kumar, 2004; Belta et al., 2005), and extend it to systems with drift. Even though other shape theoretic formation control strategies exist in literature (Zhang, 2010), this strategy was selected due its simplicity in implementation. In the following sections, μ and ς^2 have the standard definitions, $\mu = \frac{1}{N}\sum_{i=1}^{N} \mathbf{x_i}$ and $\varsigma^2 = \frac{1}{N}\sum_{i=1}^{N}(\mathbf{x_i} - \mu)'(\mathbf{x_i} - \mu)$.

3.2.1 Group behavior

In order to obtain the required behavior of the group, we employ the following control laws for the mean and the variance:

$$\dot{\mu} = K_\mu (\mathbf{x_c}(t) - \mu(t)) + \dot{\mathbf{x}}_{\mathbf{c}}(t) \tag{12a}$$
$$\dot{s} = K_s(s_d(t) - s(t)) + \dot{s}_d(t). \tag{12b}$$

where $K_\mu, K_s > 0$ and $s = \frac{N\varsigma^2}{N-1}$ is a scaled representation of the variance of the group. It is trivial to see that with these controls, $\mu(t) \to \mathbf{x_c}(t)$ and $\varsigma^2 \to \frac{N-1}{N} s_d(t)$ as $t \to \infty$, *i.e.,* we have achieved a boundary straddling formation around P_c. Now, what is left is to select $s_d(t)$ so that the spread of the grid is varied to adapt to changing flow conditions. Since our interest in this paper is on computing the FTLE field near an LCS boundary, we select s_d such that the standard deviation of the sensing grid ς, approaches the Region of Attraction (RoA) of the LCS boundary, *i.e.,* we set $s_d = \frac{N}{N-1}RoA^2$ so that $\varsigma \to RoA$ as $t \to \infty$. This will ensure that the sensing grid covers the region of attraction of the boundary and guarantee that sufficient data is available to compute the FTLE field. The details on estimating the RoA is given in appendix A.

3.2.2 Individual control laws

Once the group behavior is set, it is required to derive the control laws for individual agents based on the group behavior in a scalable manner. Belta *et al.* have shown that for a team of fully actuated, holonomic agents with the kinematics $\dot{\mathbf{x}}_\mathbf{i} = \hat{\mathbf{v}}_\mathbf{i}$, the individual control laws given by,

$$\hat{\mathbf{v}}_\mathbf{i} = \dot{\mathbf{x}}_\mathbf{i} = \dot{\mu} + \frac{\mathbf{x}_\mathbf{i} - \mu}{2s} \dot{s} \tag{13}$$

would achieve the desired group behavior specified by $\dot{\mu}$ and $\dot{s}$ (Belta and Kumar, 2004). Note that in (13), the controls for each agent is only dependent on its own state and the required group behavior and as a result the method is scalable to a large number of agents.

In contrast to Belta *et al.*, the ASVs in our case have a significant drift component in their kinematics. Therefore we use (6) to compute the control inputs (V_i and ω_i) for the ASVs in (5) as,

$$V_i = |\mathbf{V}_{\mathbf{i/f}}| \tag{14a}$$

$$\omega_i = K_{\omega_i}\left(\theta_{d_i} - \theta_i\right) + \dot{\theta}_{d_i} \tag{14b}$$

where $\mathbf{V}_{\mathbf{i/f}} = \dot{\mathbf{x}}_\mathbf{i} - \mathbf{F}(\mathbf{x}_\mathbf{i}, t)$ (from (6)), $\theta_{d_i} = \angle \mathbf{V}_{\mathbf{i/f}}$ and $\dot{\mathbf{x}}_\mathbf{i}$ is given by (13).

4 Analysis

In this section we analyze the proposed boundary tracking strategy and and the proposed formation control strategy. We show that, under certain conditions, the center agent is able to track the boundary exponentially and that the proposed formation keeping strategy is robust to measurement noise.

4.1 Tracking Strategy

In the proceeding discussion $d(\cdot, \cdot)$ denotes the Euclidean distance function and $\langle , \rangle$ denotes the inner product between two vectors.

Assumption 1 *The team of ASVs are initialized such that, $d(\mathbf{x}_\mathbf{c}(t_0), B_u) < \epsilon$ for small value of $\epsilon > 0$.*

Assumption 2 *The accuracy of the boundary location computed in (8) is such that $d(\mathbf{q}_\mathbf{h}, \mathbf{q}_\mathbf{B}) < \delta$ for a small positive value of δ where $\mathbf{q}_\mathbf{B}$ is the point on B_u that is closest to $\mathbf{q}_\mathbf{h}$.*

Assumptions 1 ensures that the ASVs are initialized in the vicinity of the boundary and that the boundary location strategies specified in Section 3.1 will initially return a valid boundary location. Assumption 2 relates to the accuracy of the boundary estimation strategies specified in Section 3.1. The value of δ will depend on the bounds of the sensor and

actuator noise, the vector interpolation routine, the spatio-temporal resolution of the flow velocity measurements, the time scales of the flow dynamics, and the inherent environmental noise.

Proposition 1 *Given a team of ASVs with kinematics given in (5), the control strategy for the center agent P_c given in (11) will ensure that $d(\mathbf{x}_\mathbf{c}(t), B_u) < D$ for $t > t_0$ for a small value of $D > 0$ if assumptions 1 and 2 are satisfied.*

Proof Let $\mathbf{q}_\mathbf{h} = \mathbf{q}_\mathbf{B} + \tilde{\mathbf{q}}$ (see Fig. 4). From Assumption 2, $|\tilde{\mathbf{q}}| < \delta$. After a time interval T_1, the perturbation term $\tilde{\mathbf{q}}$ can be written as

$$\tilde{\mathbf{q}}(t + T_1) = \phi_t^{t+T_1}(\mathbf{q}_\mathbf{h}) - \phi_t^{t+T_1}(\mathbf{q}_\mathbf{B}).$$

Due to the Lagrangian nature of LCS, $\phi_t^{t+T_1}(\mathbf{q}_\mathbf{B})$ gives a point on B_u at $t = t + T_1$ and from (9), $\hat{\mathbf{q}}_\mathbf{h} = \phi_t^{t+T_1}(\mathbf{q}_\mathbf{h})$. Therefore, $\tilde{\mathbf{q}}(t + T_1)$ represents the vector from $\hat{\mathbf{q}}_\mathbf{h}$ to a point on B_u and could be approximated as,

$$\tilde{\mathbf{q}}(t + T_1) \approx \frac{d\phi_t^{t+T_1}(\mathbf{q}_\mathbf{B})}{d\mathbf{x}} \tilde{\mathbf{q}}.$$

Thus the magnitude of this perturbation term can be written as,

$$|\tilde{q}(t + T_1)| = \sqrt{\langle \tilde{\mathbf{q}}, \Delta \tilde{\mathbf{q}} \rangle} \tag{15}$$

where Δ is the Cauchy-Green deformation tensor computed at $\mathbf{q}_\mathbf{B}$ using (4). Let the eigenvalues of Δ be λ_1 and λ_2 with $\lambda_1 < \lambda_2$ and let the corresponding normalized eigenvectors be $\mathbf{v_1}$ and $\mathbf{v_2}$. Since $\mathbf{q}_\mathbf{B}$ is on the attracting manifold, $\lambda_1 < 1 < \lambda_2$ and $\mathbf{v_2}$ would be tangent to B_u at $\mathbf{q}_\mathbf{B}$. Letting $\tilde{\mathbf{q}} = |\tilde{\mathbf{q}}|(\alpha \mathbf{v_1} + \beta \mathbf{v_2})$ with $\alpha^2 + \beta^2 = 1$, (15) can be expanded as,

$$|\tilde{q}(t + T_1)| = |\tilde{\mathbf{q}}|\sqrt{\alpha^2 \lambda_1 + \beta^2 \lambda_2 + \alpha\beta(\lambda_1 + \lambda_2)\langle \mathbf{v_1}, \mathbf{v_2}\rangle} \tag{16}$$

Using the fact that $\tilde{\mathbf{q}} = \mathbf{q}_\mathbf{h} - \mathbf{q}_\mathbf{B}$ is perpendicular to B_u at $\mathbf{q}_\mathbf{B}$, *i.e.,* $\langle \tilde{\mathbf{q}}, \mathbf{v_2}\rangle = 0$, (16) can be reduced to,

$$|\tilde{q}(t + T_1)| = |\tilde{\mathbf{q}}|\sqrt{\lambda_1(2\alpha^2 - 1)} < |\tilde{\mathbf{q}}| < \delta. \tag{17}$$

As shown in Fig. 4, $d(\hat{\mathbf{q}}_\mathbf{h}, B_u) \leq |\tilde{q}(t + T_1)| < \delta$. Therefore, it could be asserted that $d(\hat{\mathbf{q}}_\mathbf{h}, B_u) = \gamma$ with $0 < \gamma < \delta$, *i.e.,* $\hat{\mathbf{q}}_\mathbf{h}$ is closer to the boundary than $\mathbf{q}_\mathbf{h}$.

It's trivial to see that the control scheme given in (11) will lead to P_c achieving the desired speed and heading direction given in (10). This makes the heading of P_c in the inertial frame to be always directed towards $\hat{\mathbf{q}}_\mathbf{h}$. As such, $d(P_c, B_u) \to \gamma$ as $t \to \hat{t}$ for some $\hat{t} > t_0$. This together with Assumption 1 leads to $d(\mathbf{x}_\mathbf{c}(t), B_u) < D$ for $t > t_0$ where $D = \mathscr{O}(\gamma)$.
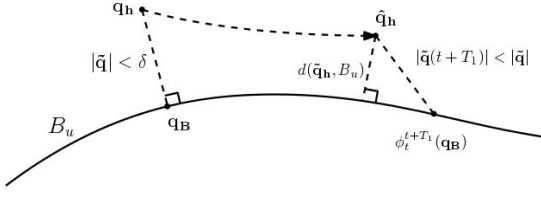
Fig. 4 The trajectory of the estimated boundary location $\mathbf{q_h}$ vs the trajectory of a point $\mathbf{q_B}$ on the actual boundary B_u

4.2 Formation Keeping

Let $\delta\mathbf{F}(t) = [\mathbf{F}(\mathbf{x_1},t) - \hat{\mathbf{F}}(\mathbf{x_1},t),...,\mathbf{F}(\mathbf{x_N},t) - \hat{\mathbf{F}}(\mathbf{x_N},t)]'$ be the error between actual and measured flow velocities, with $\hat{\mathbf{F}}(\mathbf{x_i},t)$ denoting the measurement obtained by the ith agent.

Assumption 3 *Each component of the measurement noise vector $\delta\mathbf{F}(t)$, is an independent and identically distributed (iid) ergodic random process with a normal probability distribution (Oppenheim and Verghese, 2016).*

Proposition 2 *The control laws defined in (14) exponentially achieves the desired group behavior specified by $\mathbf{x_c}$ and s_d in (12), in the presence of measurement noise $\delta\mathbf{F}$.*

Proof Let $\dot{\mu}_{\mathbf{req}}$ and $\dot{s}_{req}$ be the required controls for μ and s specified in (12) to achieve the desired group behavior $\mathbf{x_c}$ and s_d. Then from (13), the required motion for agent i is, $\dot{\mathbf{x}}_{\mathbf{req_i}} = \dot{\mu}_{\mathbf{req}} + \frac{\mathbf{x_i} - \mu}{2s}\dot{s}_{req}$. Letting $\mathbf{X} = [\mathbf{x_1}, \mathbf{x_2}, ...\mathbf{x_N}]' \in \mathbb{R}^{2N}$, this can be rewritten as,

$$\dot{\mathbf{X}}_{\mathbf{req}} = \mathbf{A}\dot{\mu}_{\mathbf{req}} + \frac{\mathbf{X} - \mathbf{A}\mu}{2s}\dot{s}_{req} \tag{18}$$

where $\mathbf{A} = [\overbrace{\mathbf{I_2}, \mathbf{I_2}, ..., \mathbf{I_2}}^{N \text{ times}}]'$ with $\mathbf{I_2}$ specifying the 2×2 identity matrix. From (6), the required velocity command for the team to achieve this required motion is,

$$[\mathbf{V_{i/f}}]_{req} = \dot{\mathbf{X}}_{\mathbf{req}} - [\mathbf{F}(\mathbf{x_1},t), \mathbf{F}(\mathbf{x_2},t), ..., \mathbf{F}(\mathbf{x_N},t)]'$$

where $[\mathbf{V_{i/f}}]_{req}$ denotes the vector of required velocity commands for the team. However, the actual velocity commands applied by the agents will depend on the measured flow velocities rather than the actual flow velocities. Thus,

$$[\mathbf{V_{i/f}}]_{act} = \dot{\mathbf{X}}_{\mathbf{req}} - [\hat{\mathbf{F}}(\mathbf{x_1},t), \hat{\mathbf{F}}(\mathbf{x_2},t), ..., \hat{\mathbf{F}}(\mathbf{x_N},t)]' \tag{19}$$

where $[\mathbf{V_{i/f}}]_{act}$ denotes the vector of velocity commands actually applied by the team. Thus, using (6), the actual motion of the team is given by,

$$\dot{\mathbf{X}} = [\mathbf{V_{i/f}}]_{act} + [\mathbf{F}(\mathbf{x_1},t), \mathbf{F}(\mathbf{x_2},t), ..., \mathbf{F}(\mathbf{x_N},t)]'$$

which, using 19, can be reduced to,

$$\dot{\mathbf{X}} = \dot{\mathbf{X}}_{\mathbf{req}} + \delta\mathbf{F} \tag{20}$$

Using the definition of μ, we can write $\dot{\mu}$ in terms of $\dot{\mathbf{X}}$ as,

$$\dot{\mu} = \frac{1}{N}\sum_{i=1}^{N}\dot{\mathbf{x}}_\mathbf{i} = \frac{\mathbf{A}'}{N}\dot{\mathbf{X}}.$$

Thus, using 18 and (20), we can write,

$$\dot{\mu} = \dot{\mu}_{\mathbf{req}} + \frac{\mathbf{A}'}{N}\delta\mathbf{F}. \tag{21}$$

Using a similar approach we can write,

$$\dot{s} = \dot{s}_{req} + \frac{\mathbf{X} - \mathbf{A}\mu'}{N-1}\delta\mathbf{F}. \tag{22}$$

To acheive the desired group behavior for the mean of the group (specified by $\mathbf{x_c}$), from (12), $\dot{\mu}_{req} = K_\mu(\mathbf{x_c} - \mu) + \dot{\mathbf{x}_c}$. Thus, (21) can be reduced to,

$$\dot{\mu} = K_\mu(\mathbf{x_c} - \mu) + \dot{\mathbf{x}_c} + \frac{\mathbf{A}'}{N}\delta\mathbf{F}.$$

Solving above, we can get the actual time variation of μ under the influence of measurement noise as,

$$\mu(t) = \mathbf{x_c}(t) + e^{-K_\mu t} + \int_0^t \frac{\mathbf{A}'}{N}\delta\mathbf{F}d\tau.$$

From Assumption 3, each component of $\delta\mathbf{F}$ is a normally distributed ergodic random process. Therefore, $\int_0^t \frac{\mathbf{A}'}{N}\delta\mathbf{F}d\tau \to 0$ as $t \to \infty$ (Oppenheim and Verghese, 2016). Thus, it can be seen that, $\mu(t) \to \mathbf{x_c}(t)$ exponentially.

Using similar constructions on (22), it can be shown that $s(t) \to s_d(t)$ exponentially.

5 Simulation Results

In this section, we validate the proposed LCS tracking strategy in simulations. The strategy is validated on 2D periodic flows given by the time dependent wind driven double gyre model, experimental 2D flow data generated in a lab setup and ocean current data obtained from the Naval Coastal Ocean Model (NCOM) database.

5.1 Time Dependent Wind Driven Double Gyre Flow

In this section we use a flow field generated using the wind-driven double-gyre flow model for the simulations. In this case, the flow is given by

$$u(\mathbf{x},t) = -\pi A \sin(\pi\frac{f(x,t)}{s})\cos(\pi\frac{y}{s}) - \mu x, \tag{23a}$$

$$v(\mathbf{x},t) = \pi A \cos(\pi\frac{f(x,t)}{s})\cos(\pi\frac{y}{s})\frac{df}{dx} - \mu y, \tag{23b}$$

$$f(x,t) = \varepsilon\sin(\omega t + \psi)x^2 + (1 - 2\varepsilon\sin(\omega t + \psi))x. \tag{23c}$$

(a) t = 31s (b) t = 38.5s
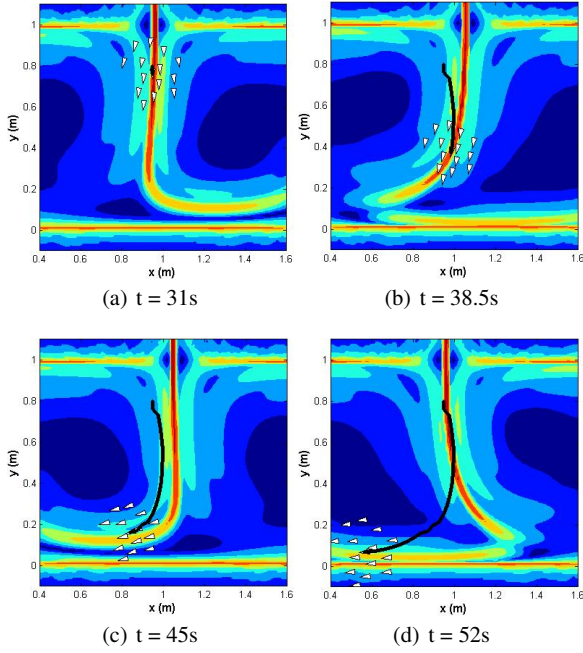
(c) t = 45s (d) t = 52s

Fig. 5 Tracking an attracting LCS in a flow generated using (23) with $A = 0.02$, $\varepsilon = 0.1$, $\omega = 2\pi/30$, $s = 1$ & $\mu = 0$

When $\varepsilon = 0$, the double-gyre flow is time-independent, while for $\varepsilon \neq 0$, the gyres undergo a periodic expansion and contraction in the x direction. In (23), A approximately determines the amplitude of the velocity vectors, $\omega/2\pi$ gives the oscillation frequency, ε determines the amplitude of the side to side motion of the separatrix between the gyres, ψ is the phase, μ determines the dissipation and s scales the dimensions of the workspace. Simulations were run with $A = 0.02$, $\varepsilon = 0.1$, $\omega = 2\pi/30$, $s = 1$ & $\mu = 0$. The flow field and the corresponding FTLE field are very similar to those shown in Fig. 2. A team of 15 ASVs was used to track an attracting LCS on this flow. Snapshots of the tracking is shown in Fig. 5, and the tracking error for this case was found to be 0.011 m.

5.2 Experimental Flow Data

The performance of the proposed tracking strategy was tested on data generated in an experimental flow tank. The tank, which is part of the multi-robot Coherent Structure Test bed (mCoSTe) at Drexel University, measures $60 \times 60 \times 30$ cm³ and is capable of generating repeatable and controllable quasi-2D flows which exhibit LCS similar to those in the ocean. A flow was generated using a 3×4 array of cylinders rotating at 60 rpm and the flow velocities were captured using a PIV system. Interested readers are referred to (Larkin, 2015) for additional information on the generation of flow data. The tank setup and a snapshot of a backward time FTLE field computed using this data is shown in Fig. 6.
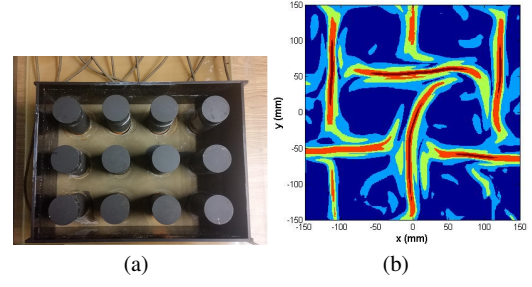

(a) (b)

Fig. 6 (a) experimental setup used to generate the data, (b) FTLE field computed from a snapshot of collected data

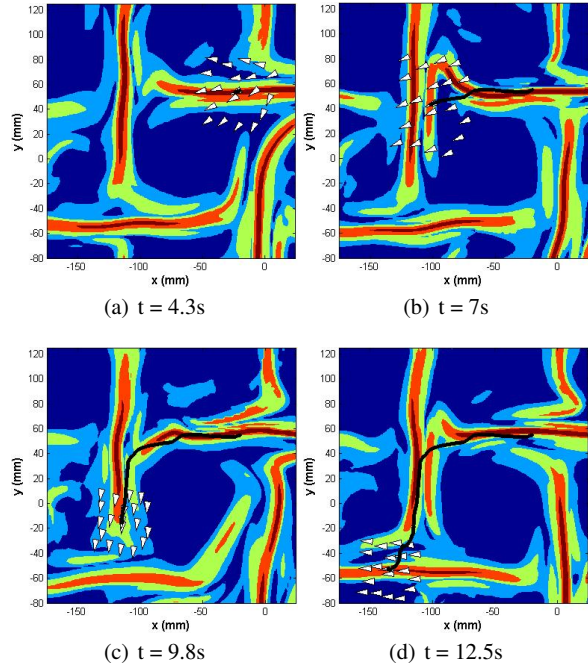(a) t = 4.3s (b) t = 7s

(c) t = 9.8s (d) t = 12.5s

Fig. 7 Tracking an attracting LCS in the experimental data generated from the flow tank

A team of 20 agents was used track attracting LCS in the captured data. Snapshots of the tracking progress is shown in Fig. 7. The tracking error for this case was found to be 1.1 mm. To asses the performance of the strategy in the presence of measurement noise, the simulation was repeated with white noise added to the velocity measurements. Three cases were considered, where the standard deviation of the noise were 5%, 15% and 20% of the mean flow velocity on the boundary. The mean performance parameters for these three cases are given in Table 1. As expected, the tracking error increases with increasing noise levels. However, considering the fact that each gyre like cell in the flow is approximately $100 \times 100mm^2$, the tracking errors are extremely small even at high noise levels. In addition, as shown in Proposition 2, the error between expected and actual group behaviors (μ and s) is relatively unaffected by noise.

Table 1 Tracking and formation keeping performance at different noise levels

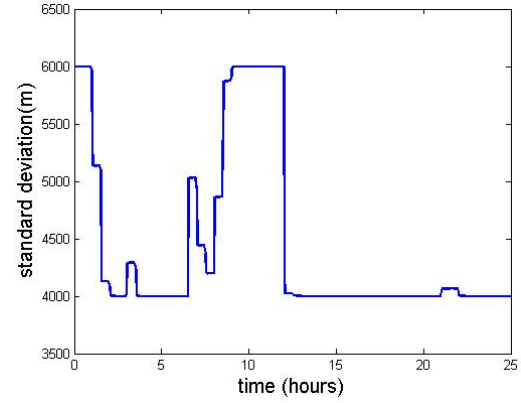| Noise %	tracking error (mm)	μ error (mm)	% s error
5	1.30	0.20	4.04
15	2.04	0.30	2.85
25	3.52	0.55	3.59

(a) (b)
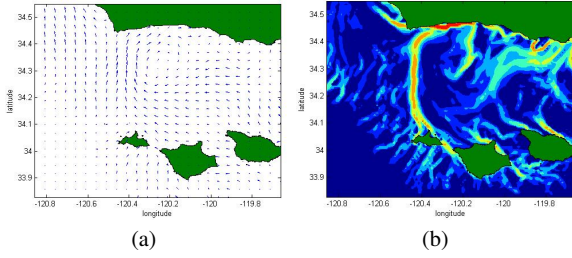
Fig. 8 (a) Time and direction reversed ocean current data for the Santa Barbara Channel for May 2012, (b) The corresponding *backward-time* FTLE field. An attracting LCS can be observed between the mainland and the San Miguel island

5.3 Ocean Data

We implemented the tracking strategy on ocean current data obtained from the Naval Coastal Ocean Model (NCOM) database hosted by the Scripps Institution of Oceanography at the University of California, San Diego (SCRIPPS, 2014).

In particular, we used ocean current data from May 2012 for the Santa Barbara Channel along the California coast. This region is instrumented with several high frequency radar stations which provide hourly surface current measurements on a 2 km grid. There is a recurring small scale eddy in this region, which results in an area of highly divergent flow between the mainland and the San Miguel island. This flow feature clearly shows up as a repelling LCS boundary in the *forward-time* FTLE field. Since our focus is on attracting LCS boundaries and since we were not able to find such a boundary in the available data, we reversed the time stamps and the flow velocity directions in the available ocean current data to convert this repelling boundary to an attracting boundary. The corresponding velocity field and the *backward-time* FTLE field are shown in Fig. 8. An attracting LCS boundary can be clearly seen extending from the San Miguel island to the mainland.

A team of 30 agents, initialized with the center agent of the grid coincident on the LCS, was used to track this LCS boundary. Snapshots of the tracking progress is shown in Fig. 10. The black line indicates the trajectory traced by the center agent P_c. The average tracking error was computed to be 92m. Fig. 9 shows the changes in standard deviation ς commanded by the strategy. Note that, the commanded standard deviation is equal to the computed RoA estimate.

Fig. 9 The standard deviation commanded by the strategy

Table 2 Tracking and formation keeping performance at different noise levels

Noise %	tracking error (m)	μ error (m)	% s error
5	129	0.6	0.144
15	462	1.3	0.139
25	539	2.4	0.166

In order to asses the performance of the strategy in the presence of measurement noise, the velocity measurements obtained by each agent were corrupted with white noise. Three cases with different standard deviations for the noise were considered. In the three cases, the standard deviations were set at 5%, 15% and 25% of the mean flow velocity along the boundary respectively. The mean performance parameters for the three cases are given in Table 2. A degradation of the tracking error can be observed with increasing noise. However, it should be noted that the spatial scales considered in these simulations are in tens of kilometers. Hence, an error of ≈ 0.5 km at high noise levels is quite satisfactory. It can also be seen that, similar to the simulations using tank data, the level of noise has little to no impact on the error between expected and actual group behaviors (μ and s).

6 Experiments

In this section we evaluate the methodology proposed in Section 3 employing our indoor laboratory experimental testbed: multirobot Coherent Structure Testbed (mCoSTe). The mCoSTe consists of a Multi Robot (MR) tank and a fleet of two types of micro-autonomous surface vehicles: the mASV and the mASVf. The proposed tracking strategy is validated using a fleet of mASVs in the MR tank. The mASVs are differential drive autonomous surface vehicles equipped with a micro-controller board, XBee radio module, and an inertial measurement unit (IMU). The vehicles are approximately 12 cm long and have a mass of about 45 g each. Localization for
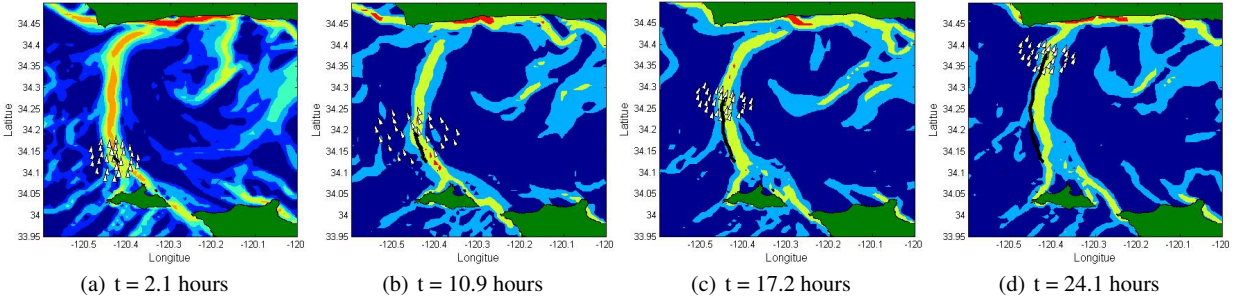
(a) t = 2.1 hours   (b) t = 10.9 hours   (c) t = 17.2 hours   (d) t = 24.1 hours

Fig. 10 Tracking an attracting LCS in the Santa Barabara channel. The black line shows the trajectory of P_c. The agents maintain a saddle straddle formation around the center agent

the mASVs is provided by an external motion capture system. The MR tank which is $3\times 3\times 1$ m^3 in size, is designed to accommodate the operation of several mASVs and is able to create time-independent flow fields that exhibit kinematic and transport features similar to those observed in the ocean. For additional details about the various components of the mCoSTe and the quality of the flows that can be created using the mCoSTe, we refer the interested reader to (Larkin et al., 2014).

Ideally, it is desirable to test the performance of the tracking strategy using real time flow velocity measurements obtained by the mASVs. However, currently the mASVs are not able to obtain flow velocity measurements that are accurate enough to carry out the necessary computations. Therefore, instead of creating an actual flow field in the the MR tank, we overlay a simulated flow field on the surface of the MR tank and obtain simulated flow velocity measurements depending on the positions of the mASVs. This also allows us to use virtual ASVs in combination with actual mASVs in the experiments.

For the experimental validation of the strategy, we employed 3 mASVs along with 7 virtual ASVs. One of the mASVs was considered to be the center agent P_c. The same flow field used for the simulations in Section 5.1 was used for the experiment. Fig. 11 shows snapshots of the tracking performance in the tank. The top row of figures ((a)-(d)), shows the positions of the sensing grid on the FTLE field of the flow field considered. The mASV functioning as the center agent is shown in green and the other three mASVs are shown in red. The virtual ASVs are shown in white. In the bottom row of figures ((e)-(h)), the simulated flow field and the virtual ASVs are overlaid on images of the mASVs in the MR tank. The virtual ASVs are represented as blue triangles and the actual mASVs can be seen in red, orange and purple. The mean tracking error in this experiment was 0.014 m which is almost the same as the tracking error in the simulations Section 5.1.

7 Conclusions and Future Work

In this work, we developed a methodology to track attracting LCS boundaries through the explicit on-board calculation of local FLTE fields. We have demonstrated how robotics systems could be used track dynamical features in a flow field that provide insights into the surrounding fluidic dynamics. The proposed method was verified in simulations using analytical flow fields as well as actual flow velocity data. In addition, the strategy was also verified using actual ASVs in an indoor laboratory testbed. Theoretical guarantees for the tracking and formation keeping strategies were also presented. We have also shown that the tracking and formation keeping strategies are robust to measurement noise.

The formation keeping strategy presented here focuses on spreading the sensing grid around the center agent such that they cover the region of attraction of the boundary. Alternatively, we could spread the grid to an optimal value, that would produce flow velocity measurements leading to the best possible FTLE computations. However, obtaining such an optimal value requires deeper analysis of the flow surrounding the LCS boundary and is a direction for future work. In addition, we would also like to verify the proposed strategy experimentally on actual flows in the MR tank. Currently work is underway to develop a method to obtain real time flow velocity measurements from the MR tank, that would facilitate such an experiment.

A Estimating the Region of Attraction

In this section, we describe the methodology used to estimate the Region of Attraction (RoA) of the boundary. This estimate for the RoA is used in 3.2 to set the desired group behavior of the sensing grid.

Even if we had an analytical description for the flow field, obtaining a closed form expression for the RoA is extremely difficult. In the case of a discrete representation of the flow field (in the form of sparse velocity measurements), we have no other option but to estimate the RoA numerically. To do this, we consider the flow velocities of a set of points along a perpendicular line segment across the boundary through P_c (see Fig. 12(a)). The length of the line segment (l) is selected to be $2 \times \varsigma$, so that it extends a distance of ς on either side of the boundary. (Note that ς is the standard deviation of the sensing grid). Due to the

(a) t = 0s   (b) t = 7.8s   (c) t = 16.4s   (d) t = 22.9s

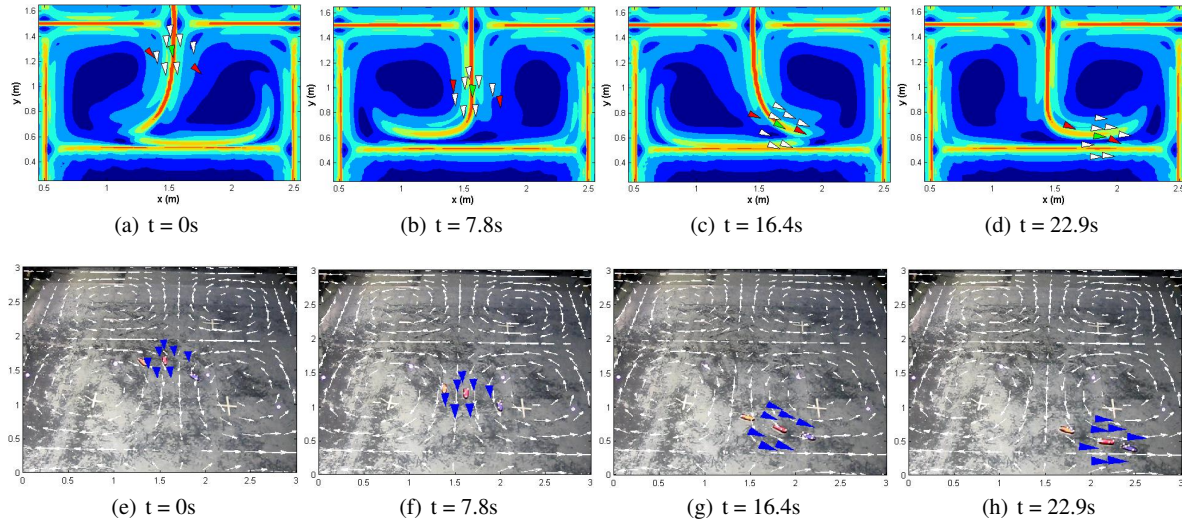(e) t = 0s   (f) t = 7.8s   (g) t = 16.4s   (h) t = 22.9s

Fig. 11 (a)-(d) The positions of the sensing grid overlaid on top of the FTLE field of the simulated flow. The green triangle shows the position of the mASV functioning as the center agent while the other mASVs are shown as red triangles. The virtual ASVs are shown in white. (e)-(h) shows the simulated flow and the virtual ASVs (blue) overlaid on the surface of the MR tank. The actual mASVs can be seen in red (P_c), orange and purple

attractive nature of the boundary, the flow speed components on this line, towards the boundary, typically has the distribution shown in Fig. 12(b). The flow speed towards the boundary increases on either side of the boundary as we move away from it and then tapers off as we approach the edge of the attracting region. Thus, as shown in Fig. 12(b), we approximate RoA as,

$$RoA = max(\|\mathbf{x_{m1}} - \mathbf{x_c}\|, \|\mathbf{x_{m2}} - \mathbf{x_c}\|)$$

where $\mathbf{x_{m1}}, \mathbf{x_{m2}}$ are the points on the line on either side of the boundary having the maximum normal flow. If the maximum normal flows are at either end of the line, that indicates that the RoA is larger than $l/2$, *i.e.*, $RoA > \varsigma$ (see Fig. 12(c)). Therefore, on such instances we set

$$RoA = \alpha \times \varsigma$$

where $\alpha > 1$.

References

Belta, C. and Kumar, V. Abstraction and control for groups of robots. *Robotics, IEEE Transactions on*, 20(5):865–875, 2004.

Belta, C., Pereira, G., and Kumar, V. Abstraction and control for swarms of robots. In *Robotics Research. The Eleventh International Symposium*, volume 15, pages 224–233. Springer Berlin Heidelberg, 2005.

Forgoston, E., Billings, L., Yecko, P., and Schwartz, I. B. Set-based corral control in stochastic dynamical systems: Making almost invariant sets more invariant. *Chaos*, 21(013116), 2011.

Haller, G. A variational theory of hyperbolic lagrangian coherent structures. *Physica D*, 240:574–598, 2011.

Haller, G. and Yuan, G. Lagrangian coherent structures and mixing in two-dimensional turbulence. *Phys. D*, 147:352–370, December 2000. ISSN 0167-2789. doi: 10.1016/S0167-2789(00)00142-1. URL http://dl.acm.org/citation.cfm?id=366463. 366505.

Harrison, C. S. and Glatzmaier, G. A. Lagrangian coherent structures in the california current system sensitivities and limitations. *Geophysical & Astrophysical Fluid Dynamics*, 106(1):22–44, 2012.

Heckman, C. R., Hsieh, M. A., and Schwartz, I. B. Controlling basin breakout for robots operating in uncertain flow environments. In *International Symposium on Experimental Robotics (ISER 2014)*, Marrakech/Essaouira, Morocco, June 2014.

Hsieh, M. A., Forgoston, E., Mather, T. W., and Schwartz, I. Robotic manifold tracking of coherent structures in flows. In *Proc. IEEE Int. Conf. on Robotics and Automation (ICRA2012)*, Minneapolis, MN USA, May 2012.

Hsieh, M. A., Mallory, K., and Schwartz, I. B. Distributed allocation of mobile sensing agents in geophysical flows. In *Proc. of the 2014 American Controls Conference*, Portland, OR, 2014.

Inanc, T., Shadden, S., and Marsden, J. Optimal trajectory generation in ocean flows. In *American Control Conference, 2005. Proceedings of the 2005*, pages 674 – 679, 8-10, 2005. doi: 10.1109/ACC.2005. 1470035.

Kularatne, D. and Hsieh, M. A. Tracking attracting lagrangian coherent structures in flows. In *Proceedings of Robotics: Science and Systems*, Rome, Italy, July 2015.

Larkin, D., Michini, M., Abad, A., Teleski, S., and Hsieh, M. A. Design of the multi-robot coherent structure testbed (mcoste) for distributed tracking of geophysical fluid dynamics. In *ASME International Design Engineering Technical Conferences (IDETC)*, Buffalo, NY USA, Aug 2014.

Larkin, D. J. An experimental testbed for creating controlled lagrangian coherent structures. Master's thesis, Drexel University, 2015.

Lermusiaux, P. and Lekien, F. Dynamics and lagrangian coherent structures in the ocean and their uncertainty. In *Dynamical System Methods in Fluid Dynamics, Oberwolfach Workshop*. Mathematisches Forschungsinstitut Oberwolfach, 2005.

Mallory, K., Hsieh, M. A., Forgoston, E., and Schwartz, I. B. Distributed allocation of mobile sensing swarms in gyre flows. *Nonlin. Processes Geophys.*, 20(5):657–668, 2013.

Michini, M., Hsieh, M. A., Forgoston, E., and Schwartz, I. B. Robotic tracking of coherent structures in flows. *IEEE Trans. on Robotics*, 30(3):593–603, 2014a.

Michini, M., Hsieh, M. A., Forgoston, E., and Schwartz, I. B. Experimental validation of robotic manifold tracking in gyre-like flows. In *Proc. IEEE/RSJ International Conference on Intelligent Robots and*
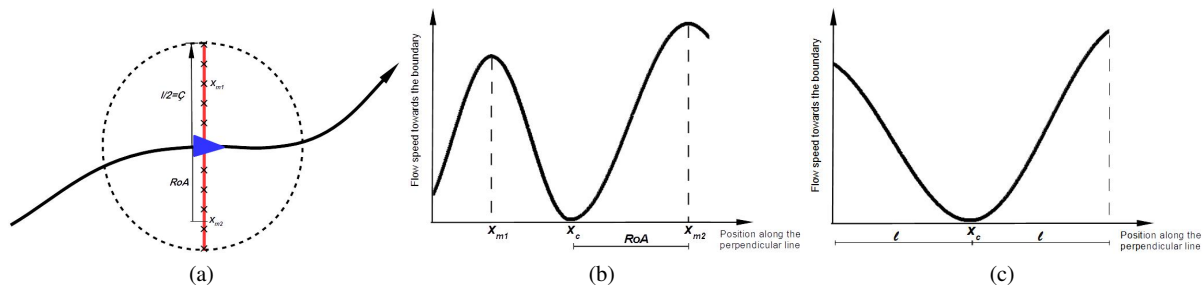
Fig. 12 (a) The red line shows the line segment perpendicular to the boundary through P_c. The length of the line is 2ς, (b) The flow speed directed towards the boundary on the line segment. Two maximums on either side of the boundary, (c) Maximums flow speeds are on the edges of the line, *i.e.,* the line segment is not long enough to capture the RoA

Systems (IROS) 2014, Chicago, IL USA, Sep 2014b.

Michini, M., Rastgoftar, H., Hsieh, M. A., and Jayasuriya, S. Distributed formation control for collaborative tracking of manifolds in flows. In *Proc. of the 2014 American Control Conference (ACC 2014)*, Portland, OR, Jun 2014c.

Nusse, H. E. and Yorke, J. A. A procedure for finding numerical trajectories on chaotic saddles. *Physica D Nonlinear Phenomena*, 36: 137–156, jun 1989. doi: 10.1016/0167-2789(89)90253-4.

Olascoaga, M. J., Beron-Vera, F. J., Brand, L. E., and Koak, H. Tracing the early development of harmful algal blooms on the west florida shelf with the aid of lagrangian coherent structures. *Journal of Geophysical Research*, 113(c12):c12014–, 2008.

Olascoaga, M. J. and Haller, G. Forecasting sudden changes in environmental pollution patterns. *Proceedings of the National Academy of Sciences*, 109(13):4738–4743, 2012.

Oppenheim, A. and Verghese, G. C. *Signals, systems and inference*. Pearson, Boston, 2016.

SCRIPPS. Naitonal HF RADAR network - surface currents, 2014. URL http://cordc.ucsd.edu/projects/mapping/maps/.

Senatore, C. and Ross, S. Fuel-efficient navigation in complex flows. In *American Control Conference, 2008*, pages 1244 –1248, june 2008. doi: 10.1109/ACC.2008.4586663.

Shadden, S. C., Lekien, F., and Marsden, J. E. Definition and properties of lagrangian coherent structures from finite-time lyapunov exponents in two-dimensional aperiodicflows. *Physica D: Nonlinear Phenomena*, 212(3-4):271 – 304, 2005. ISSN 0167-2789. doi: DOI:10.1016/j.physd.2005.10.007.

Shchepetkin, A. and McWilliams, J. Quasi-monotone advection schemes based on explicit locally adaptive dissipation. *Monthly Weather Review*, 126:1541–1580, 1998.

Shchepetkin, A. F. and McWilliams, J. C. The regional oceanic modeling system (roms): a split-explicit, free-surface, topography-following-coordinate oceanic model. *Ocean Modeling*, 9:347–404, 2005.

Smith, R. N., Chao, Y., Li, P. P., Caron, D. A., Jones, B. H., and Sukhatme, G. S. Planning and implementing trajectories for autonomous underwater vehicles to track evolving ocean processes based on predictions from a regional ocean model. *International Journal of Robotics Research*, 29(12):1475–1497, 2010. doi: http://dx.doi.org/10.1177/0278364910377243.

Zhang, F. Geometric cooperative control of particle formations. *IEEE Transactions on Automatic Control*, 55(3):800–803, March 2010. ISSN 0018-9286. doi: 10.1109/TAC.2010.2040508.